LA-UR-17-31124 (Accepted Manuscript)

Validation of micro-mechanical FFT-based simulations using High Energy Diffraction Microscopy on Ti-7Al

Tari, Vahid
Lebensohn, Ricardo A.
Pokharel, Reeju
Turner, Todd
Shade, Paul
Bernier, Joel
Rollett, Anthony

To be published in: Acta Materialia

DOI to publisher's version: 10.1016/j.actamat.2018.05.036

Permalink to record: http://permalink.lanl.gov/object/view?what=info:lanl-repo/lareport/LA-UR-17-31124

Accepted Manuscript

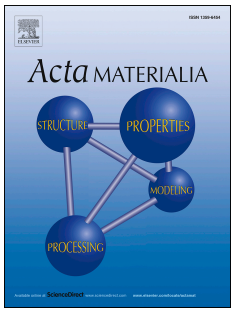

Validation of Micro-Mechanical FFT-based Simulations using High Energy Diffraction Microscopy on Ti-7Al

Vahid Tari, Ricardo A. Lebensohn, Reeju Pokharel, Todd J. Turner, Paul A. Shade, Joel V. Bernier, Anthony D. Rollett

PII: S1359-6454(18)30396-3

DOI: 10.1016/j.actamat.2018.05.036

Reference: AM 14589

To appear in: *Acta Materialia*

Received Date: 26 March 2018

Revised Date: 15 May 2018

Accepted Date: 16 May 2018

Please cite this article as: V. Tari, R.A. Lebensohn, R. Pokharel, T.J. Turner, P.A. Shade, J.V. Bernier, A.D. Rollett, Validation of Micro-Mechanical FFT-based Simulations using High Energy Diffraction Microscopy on Ti-7Al, *Acta Materialia* (2018), doi: 10.1016/j.actamat.2018.05.036.

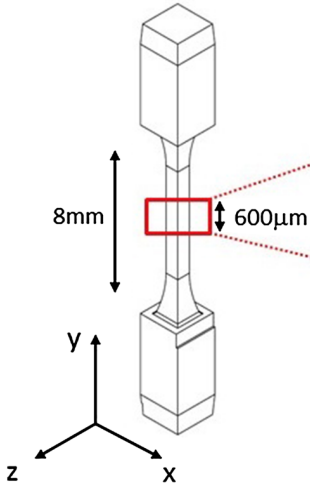

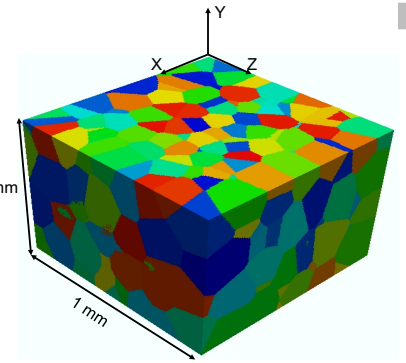

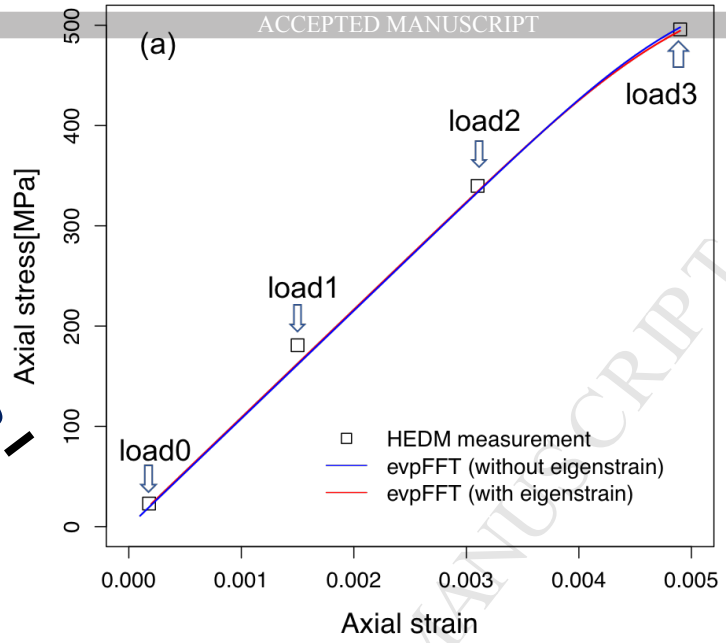

Grain scale comparison at load 0

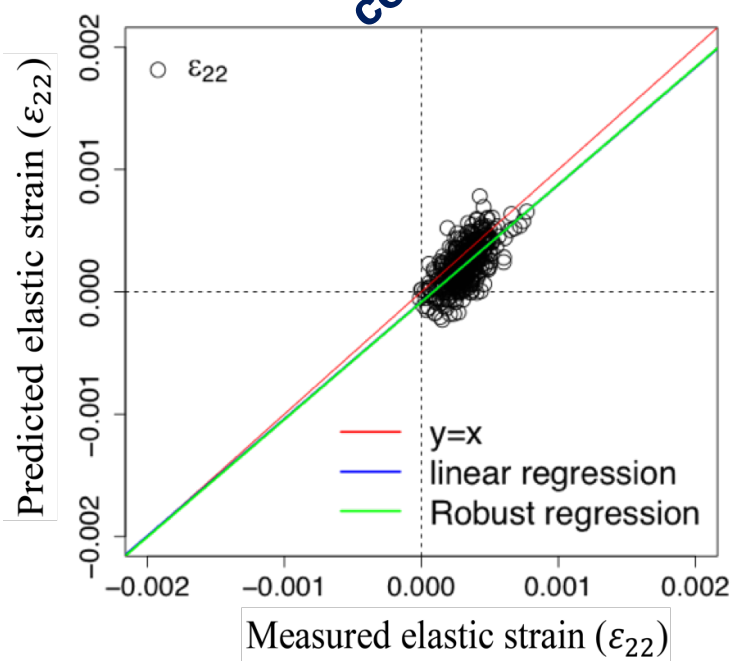

Grain scale comparison at load 0

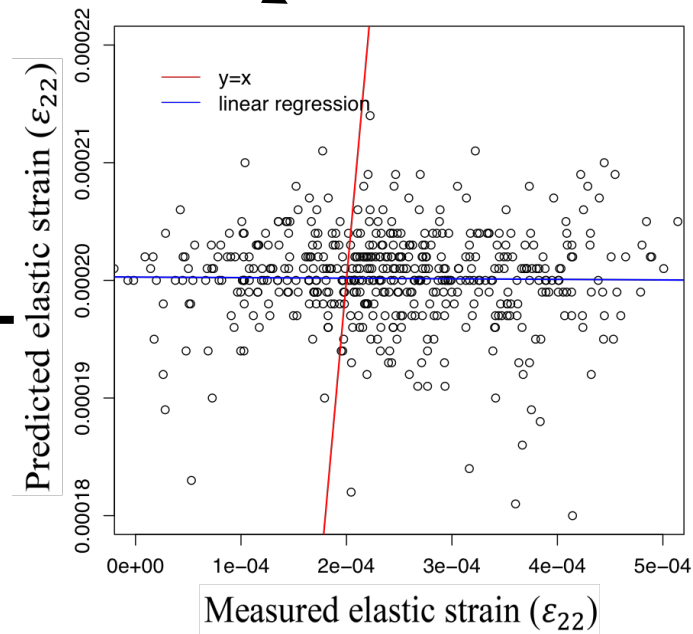

New simulation was instantiated by Eigenstrain

Validation of Micro-Mechanical FFT-based Simulations using High Energy Diffraction Microscopy on Ti-7Al

Vahid Tari[a] , Ricardo A. Lebensohn[b], Reeju Pokharel[b] Todd J. Turner[c], Paul A. Shade[c], Joel V. Bernier[d], Anthony D. Rollett[a]

[a] Department of Materials Science and Engineering, Carnegie Mellon University, Pittsburgh, PA 15213, USA
[b] Los Alamos National Laboratory, Los Alamos, NM 87545, USA
[c] Air Force Research Laboratory, Wright-Patterson AFB, OH 45433, USA
[d] Lawrence Livermore National Laboratory, Livermore, CA 94550, USA

Abstract

A validation is reported for micromechanical simulation using a reimplementation of an elasto-viscoplastic FFT-based (EVPFFT) formulation, i.e., the Micromechanical Analysis of Stress-strain Inhomogeneities with fast Fourier transform (MASSIF) code, against experimental data obtained from synchrotron x-ray diffraction. The experimental data was collected during in-situ deformation of a titanium alloy specimen by High Energy Diffraction Microscopy (HEDM), which provided the average elastic strain tensor and orientation of each grain in a polycrystalline sample. MASSIF was used to calculate the local micromechanical fields in a Ti-7Al polycrystalline sample at different load levels. The initially attempted simulation showed that, although the effective response was calibrated to reproduce the experiment, MASSIF was not able to reproduce the micromechanical fields at the scale of individual grains. The differences between calculated and measured averages at the grain scale were related to initial residual strains resulting from the prior processing of the material, which had not been incorporated in the original calculation. Accordingly, a new simulation was instantiated using information on the measured residual strains to define a set of eigenstrains, calculated via an Eshelby approximation. This initialization significantly improved the correlation between calculated and simulated fields for all strain and stress components, for measurements performed within the elastic regime. For the measurements at the highest load, which was past plastic yield, the correlations deteriorated because of plastic deformation at the grain level and the lack of an accurate enough constitutive description in this deformation regime.

1. Introduction

Failure is the most general limitation in engineering applications of polycrystalline materials. In the absence of macroscopic stress concentrations, damage nucleation usually originates from deformation heterogeneities at the intergranular scale. Experimental techniques have been widely used to capture local heterogeneities in polycrystalline materials in an attempt to identify the regions where damage is most likely to nucleate [1]. While these experimental methods, including both in-situ and ex-situ measurements, are costly and time consuming, mesoscale modeling applied to engineering design can be a faster alternative. However, in order to apply mesoscale simulations to design novel materials, these models must be rigorously validated against experimental evidence at the relevant length scales.

The validation of mesoscale modeling is usually performed by comparison with micromechanical measurements of attributes such as local strain fields, local crystallographic texture, and evolving shape of grains. Digital image correlation (DIC) is a common technique to measure local total (elastic + plastic) strain fields calculated from the relative displacement of points on the surface of a sample during deformation [2,3]. EBSD is another useful and common method utilized for model validation, by which the evolving shapes and orientations of grains on a surface during deformation are determined [4–6]. Nevertheless, DIC and EBSD only provide information from the surface of the sample, while sub-surface microstructural information is not accessible without serial sectioning. Serial sectioning combined with EBSD, known as 3D-EBSD, provides information on the three-dimensional (3D) microstructure and shape of grains [7–9]. However, the destructive nature of 3D-EBSD means that only the final state of the sample can be evaluated; model validation studies that utilize an experimentally measured microstructure must therefore be limited to small amounts of deformation [10]. It also means repeated scans of the same volume to assess the evolution of micromechanical state are not possible.

High-Energy Diffraction Microscopy (HEDM) – an in-situ and a non-destructive experimental technique – can provide simultaneous measures of the microstructure and micromechanical state for $O(10^3)$ grains comprising a mesoscopic volume during deformation [11–13]. Far-field HEDM (ff-HEDM) provides average orientations, elastic strain tensors, centroidal coordinates, and relative volumes on a per-grain basis [14–16], while near-field HEDM (nf-HEDM) provides spatially-resolved crystallographic orientation maps, which reveal both grain morphology as well as intragranular misorientation [17,18]. Pokharel *et al*. [1] showed that mesoscale models can successfully predict global quantities such as effective stress, strain, and crystallographic texture, whereas agreement deteriorates between the predicted inter- and intragranular fields and those measured by HEDM. Turner *et al*. [19] performed crystal plasticity Finite Elements (CP-FEM) simulations on a virtual microstructure instantiated from an HEDM measurement to predict local micromechanical fields in a Ti-7Al specimen subjected to tensile deformation. The

results showed good agreement for the changes in elastic strain as a function of loading, but the simulation was not able to accurately reproduce the intergranular stresses. They concluded that the lack of consideration of the initial residual stress in the material was the main source of disagreement between calculated and simulated results. One of the key contributions of this work is to show that the incorporation of the initial residual stress distribution allows for better predictions of the intergranular strain values following deformation.

Grain-level residual stresses may be produced in a material as a result of thermomechanical processing history [20] and have been previously observed in Ti-7Al [21] as well as other materials [16,22] using ff-HEDM. The use of ff-HEDM to measure the initial residual stress state allows for the opportunity to incorporate this information into mesoscale modeling. In this work, we utilize HEDM data of Ti-7Al measured by Turner *et al*. [23], and use the Micromechanical Analysis of Stress-Strain Inhomogeneities with fast Fourier transforms (MASSIF) code, which is a parallelized version of the original elasto-viscoplastic FFT-based (EVPFFT) code [24] with Hierarchical Data Format (HDF) input/output [25], to simulate the uniaxial tension test. This is done in combination with the method developed by Pokharel and Lebensohn [26] to instantiate the initial state of residual stresses in the micromechanical simulations. Next, we compare qualitatively and quantitatively the calculated micromechanical fields with the measured ones at grain scale for different macroscopic applied load levels, and describe the effect of residual stress on the predicted micromechanical fields. Finally, we discuss potential sources for the differences between calculated and measured fields at the grain scale.

2. Materials and Methods

As mentioned above, this work uses the results of an experiment performed by Turner *et al*. [19,23], in which microstructure and micromechanical fields in a single α-phase (HCP structure) titanium alloy (Ti-7Al) under tensile loading were characterized in-situ. This material is an interesting candidate for HEDM measurements and corresponding mesoscale modeling because of its elastic and plastic anisotropy. The cast material was subjected to thermomechanical processing [19,23] to obtain a single α-phase microstructure with ~100 μm average grain size and strong basal texture parallel to the direction 3 as shown in Fig. 1(a). The tensile sample was mounted with the tensile axis parallel to the direction 2 with respect to the sample reference frame.

Before applying any mechanical loading, initial ff-HEDM was performed to measure the centroid, orientation, and initial elastic strain tensor in each grain, and nf-HEDM to map the orientation field in the central portion of the sample. Fig. 1(b) shows the measured ff-HEDM dataset in three dimensions. The three-dimensional microstructure used as input for our simulations was constructed by Voronoi tessellation using the measured grain centroid

positions as seeds. The ff-HEDM data set contains 550 grains in a unit cell with dimensions of $200 \times 150 \times 200$ voxels. Fig. 1(c) shows the grain morphologies of 69 grains in the central region of the far field volume where nf-HEDM data was available (detailed information of this experiment can be found in [23]). Although initial ff-HEDM measurements were sought in an unloaded state, there was in fact a small axial loading of 23 MPa that resulted from the procedure of mounting the sample in the grips. This point will be extensively discussed in the initial Eigenstrain field section.

To further measure the elastic strain tensor in each grain at different load levels, uniaxial loading was applied on the tensile sample up to three different loads, designated as *load 1, load 2*, and *load 3* in Fig. 2(a), and ff-HEDM measurements were performed at each load. In the course of performing the analysis for this work, several errors were discovered in the published data archive [23]. First, the entry in the HDF5 archive for load 3 was found to be a duplicate of load 2. Second, a critical figure of merit for ranking the grains – discussed further below – was omitted. With the aim of facilitating future studies, Bernier, Shade, and Turner plan to submit an erratum to correct these issues, and also provide a more detailed description of the critical parameters used in the data reduction.

There are two steps to the ff-HEDM analysis used to generate the grain-based data in [23]: a) indexing, in which orientations are assigned to the measured intensities in the rotation series; and b) subsequent fitting, in which parameters for orientation (3), center-of-mass coordinates (3), and lattice stretch (6) are optimized for each orientation (grain) for a total of 12 parameters. Each step has an associated figure of merit used to cull and rank the results. For indexing, the figure of merit is “completeness” – the ratio of expected to predicted diffraction signals above a specified threshold and within a specified angular tolerance. The completeness serves as a minimum threshold of acceptance for an orientation to be labeled as a valid grain, and several factors must be considered in defining a suitable threshold. In general, the indexing process uses the first 5-6 Bragg reflections having the highest structure factor to avoid biasing out small grains. For these data, the minimum completeness was defined over the first five HCP reflections as 67 %, which yielded 605 orientations. Each orientation is subsequently fit using a forward-projection method to extract the associated diffracted beam vectors [15], yielding three components for each observed reflection over a minimum intensity threshold [15]. Fitting is typically performed over a larger range of reciprocal space than (orientation) indexing for additional strain resolution; in this case all reflections up to ~0.68 Å, which on average yielded ~75 reflections per grain. The 12 grain parameters are optimized in a non-linear least squares problem formulated over the predicted and measured diffracted beam vector components. Accordingly, the objective function that is minimized is the sum of squared residuals, which are computed as the differences between the measured and calculated reciprocal lattice vectors for each grain. The final figure of merit for ranking grains post-refinement is defined as the sum of squared residuals of diffracted beam vector coordinates normalized by the total number of

degrees of freedom in the fit (i.e., the number of measured diffracted beam vector components divided by 12). There are many causes for grains with otherwise high completeness to have poor post-refinement figures of merit in ff-HEDM data reduction, the most common being due to overlapped reflections and/or reflections with a large angular extent resulting from substantial intragranular misorientation. It is also possible for a small number of spurious orientations to persist through the indexing step. For this reason, the criterion for including a grain for comparison to simulated results is for the normalized sum of squared residuals to be $\leq 10^{-3}$. This culls the original 605 orientations down to 550 valid grains.

3. Micromechanical Model

A polycrystalline material is an aggregate of grains with different orientations. The difference in orientation between neighboring grains combined with the anisotropic elastic and plastic single crystal response causes local heterogeneities at the grain scale when the polycrystalline material is subjected to an external loading. These local heterogeneities can be the source of localized stress/strain regions in the microstructure, and consequently facilitate damage nucleation at the grain scale [27]. To predict local micromechanical fields at the grain scale, we use MASSIF code, which is based on the elasto-viscoplastic fast Fourier transform-based (EVPFFT) model of Lebensohn *et al* [24]. The FFT-based formulation, originally developed by Moulinec and Suquet [28] for linear composites, was improved by Michel *et al*. [29] in terms of its numerical convergence, to allow accurate prediction of local micromechanical fields in non-linear composites. Lebensohn *et al*. [24] developed an elasto-viscoplastic version of the latter formulation for micromechanical predictions of plastically-deforming polycrystals. FFT-based methods use input from an image of the initial microstructure discretized on a regular grid, and calculate local strain and stress fields at each grid point that respectively fulfill equilibrium and compatibility, under the applied boundary conditions. EVPFFT/MASSIF is based on small strain kinematics [24] (a simplified assumption whose adoption is justified in this case due to the relatively small plastic deformation—even at the highest load—and, consequently, very minor lattice rotations) and uses the following constitutive relation between local strain and stress:

$$\varepsilon_{ij}(x) = \varepsilon_{ij}^{e}(x) + \varepsilon_{ij}^{p}(x) = C_{ijkl}^{-1}(x)\sigma_{kl}(x) + \varepsilon_{ij}^{p,t}(x) + \dot{\varepsilon}_{ij}^{p}(x,\sigma)\Delta t \quad (1)$$

where $\varepsilon_{ij}(x)$ is the local total strain at each grid point x, and is calculated as summation of the local elastic strain $\varepsilon_{ij}^{e}(x)$ and local plastic strain $\varepsilon_{ij}^{p}(x)$. Elastic strain is computed via Hooke's law at each point. Plastic strain after each time increment Δt, is calculated based on an Euler discretization for the time integration of the local plastic strain rate, which is given by:

$$\dot{\varepsilon}_{ij}^{p}(x) = \dot{\gamma}_0 \sum_{s=1}^{Ns} m_{ij}^{s}(x) \left(\frac{|m_{kl}^{s}(x)\sigma'_{kl}(x)|}{\tau^{s}(x)} \right)^{n} \times sgn(m_{kl}^{s}(x)\sigma'_{kl}(x)) \quad (2)$$

where $\dot{\gamma}_0$ is a reference shear rate, N_s is the total number of slip systems, m^s is the symmetric Schmid tensor for each slip system, σ' is the deviatoric stress tensor, τ^s is the critical resolved shear stress (CRSS) in slip system s, and n is the rate-sensitivity exponent. The local CRSS and Schmid tensor are updated at the end of each strain step. The evolution of local CRSS at each point is calculated in this work by the Voce hardening law given by:

$$\Delta\tau^{\alpha} = \frac{d\bar{\tau}^{\alpha}}{d\Gamma} \sum_{\beta} h^{\alpha\beta}\, \dot{\gamma}^{\beta} \quad (3)$$

$$\bar{\tau}^{\alpha} = \tau_0 + (\tau_1 + \theta_1\Gamma)\left[1 - \exp\left(-\frac{\theta_0\Gamma}{\tau_1}\right)\right] \quad (4)$$

Based on this, the hardening rate, $\frac{d\bar{\tau}^{\alpha}}{d\Gamma}$, for each slip system is given by:

$$\frac{d\bar{\tau}^{\alpha}}{d\Gamma} = \theta_1 + \left(\left|\frac{\theta_0}{\tau_1}\right|\tau_1 - \theta_1\right) exp\left(-\Gamma\left|\frac{\theta_0}{\tau_1}\right|\right) + \left|\frac{\theta_0}{\tau_1}\right|\theta_1\Gamma exp\left(-\Gamma\left|\frac{\theta_0}{\tau_1}\right|\right) \quad (5)$$

where τ^{α} is the critical resolved shear stress in slip system α, $h^{\alpha\beta}$ is the latent hardening showing how slip activity in slip system β harden the occurrence of slip in slip system α, $\dot{\gamma}^{\beta}$ is the shear rate of slip on system β, Γ is the accumulated slip across all slip systems, and $\tau_0, \tau_1, \theta_0, \theta_1$ are the Voce hardening law parameters.

The current MPI implementation of MASSIF implements reading and writing data with parallel HDF libraries [25], which significantly increases the overall speed of simulations. The current simulation on a grid with $216 \times 150 \times 216$ points required a total time of 446 seconds per each strain step using 54 processors on Bridges at the Pittsburgh Supercomputing Center, of which reading the input image and writing the output fields required 0.633 and 2.304 seconds, respectively.

4. Simulation Instantiation

In order to compute local micromechanical fields in the Ti-7Al alloy, we performed MASSIF simulations under uniaxial tension along the direction 2 on the measured ff-HEDM volume. We padded the HEDM microstructure with an 8-voxel buffer zone that has infinite compliance [30] in the direction 1 and direction 3; the calculation is thus periodic from a numerical point of view

but the loaded material is isolated in the directions 1 and 3. In direction 2, however, the top and bottom ends are in (periodic) contact, but a previous study [31] suggests that the errors introduced in the local fields by this spurious contact die down a few layers away from that location and have little impact on the overall results.

4.1 Initial Eigenstrain Field

If the undeformed material contains residual stresses, these need to be considered as the initial condition of the micromechanical calculation. The residual stresses are measured via ff-HEDM as an elastic strain tensor in each grain. To approximate the initial micromechanical state in the material, these measured strains are converted to eigenstrains on a per-grain basis, which are then equilibrated in the first step of the simulation, to (ideally) reproduce the measured average elastic strains in the grains. For this, Eq. (1) was expanded by Pokharel and Lebensohn [26] to include a set of eigenstrains $\varepsilon_{ij}^{*}(x)$ to give:

$$\varepsilon_{ij}(x) = \varepsilon_{ij}^{e}(x) + \varepsilon_{ij}^{p}(x) + \varepsilon_{ij}^{*}(x) = C_{ijkl}^{-1}(x)\sigma_{kl}(x) + \varepsilon_{ij}^{p,t}(x) + \dot{\varepsilon}_{ij}^{p}(x,\sigma)\Delta t + \varepsilon_{ij}^{*}(x) \quad (6)$$

The first step in the method presented in [26] gives an initial approximation of the relation between a uniform eigenstrain in each grain (i.e. $\varepsilon_{ij}^{*}(x) = \varepsilon_{ij}^{*,g}$), and the measured average elastic strain $\varepsilon_{ij}^{e,g}$ in the grain, using the following relation:

$$\varepsilon_{ij}^{*,g} = (S_{ijkl} - I_{ijkl})^{-1}\varepsilon_{kl}^{e,g} \quad (7)$$

where S_{ijkl} is the Eshelby tensor, and I_{ijkl} is the fourth-rank identity matrix. The Eshelby tensor is computed using the numerical solution given by Lebensohn *et al*. [32]. As noted above, the intention of introducing these eigenstrains is to obtain upon equilibration an elastic strain field whose grain averages match the measured residual elastic strains in the grains.

While the ideal case corresponds to an unloaded state so that the initial strains are purely internal, the initial measurements for the Ti-7Al specimen were performed under a 23 MPa axial loading, due to limitations of the loading system used at the time. Thus, an additional challenge in this work was to consider the macroscopic contribution to the internal elastic strain in the initial state. To this end, we computed the average elastic strain tensor imposed by the applied 23 MPa at *load 0* as:

$$E_{ij} = \frac{\sum \varepsilon_{ij}^{e,g}}{N_1 \times N_2 \times N_3} \quad (8)$$

where E_{ij} is the average of the elastic tensor in the ff-HEDM dataset, $\sum \varepsilon_{ij}^{e,g}$ is the summation of the elastic tensor measured by ff-HEDM, and $N_1 \times N_2 \times N_3$ is the total number of points in the ff-HEDM volume, not including the buffer points. Then, the initial residual elastic tensor in each grain used in the eigenstrain calculation, Eq. (6), is given by:

$$\varepsilon_{ij}^{r,g} = \varepsilon_{ij}^{e,g} - E_{ij} \tag{9}$$

where $\varepsilon_{ij}^{r,g}(x)$ is the initial residual elastic strain at each point, and $\varepsilon_{ij}^{e,g}(x)$ is the measured elastic strain tensor in each grain at *load 0*.

As shown in [26], the instantiation of eigenstrains using Eq. 6 gives imperfect correlation between the calculated average elastic strains in the grains and those measured by HEDM at *load 0*. Therefore, a symmetric adjustment matrix β_{ij}, which should be determined from the data by means of the methodology further described in [26], is used to improve the initial correlation at *load* 0, as follows:

$$\varepsilon_{ij}^{*,g} = \beta_{ij}(S_{ijkl} - I_{ijkl})^{-1}\varepsilon_{kl}^{r,g} \qquad \text{(no sum over ij)} \tag{10}$$

5. Results

Figure 2(a) shows the macroscopic stress-strain curve calculated by MASSIF using the elastic stiffness matrix [33] and calibrated Voce hardening parameters from a different study of Ti-7Al, in which the material was deformed beyond the elastoplastic transition into the fully-plastic regime [34] given in table 1 and table 2, respectively. The *load 1* and *load 2* points are on the same straight line from the origin whereas *load 3* point deviates from linearity, indicating that the material had already undergone some degree of plastic deformation.

As mentioned before, HEDM measures a grain-averaged elastic strain tensor for each grain, and consequently a single stress tensor is deduced from the measured elastic tensor in each grain using Hooke's law:

$$\sigma_{ij}^{g} = C_{ijkl}^{s}\varepsilon_{kl}^{e,g} \tag{11}$$
$$C_{ijkl}^{s} = g_{im}^{-1}g_{jn}^{-1}g_{kp}^{-1}g_{lq}^{-1}C_{mnpq}^{c}$$

where σ_{ij}^{g} and $\varepsilon_{kl}^{e,g}$ are the stress tensor and the measured elastic strain tensor in each grain, expressed in the sample reference frame, respectively. C_{ijkl}^{s} is the elastic stiffness tensor in the sample reference frame, and C_{mnpq}^{c} is the elastic stiffness tensor in the crystal reference frame given in table 1. g_{ij} is the orientation matrix of each grain with respect to the sample reference frame.

Neither the measured elastic strain nor the deduced stress tensors reflect the local intragranular variations in strain and stress in each grain caused by the neighboring grains. Therefore, in order to compare the grain-averaged quantities measured by HEDM with the model predictions, we took the average value of the calculated stress/strain fields in each grain by linear addition of the local stress/strain tensorial components in each voxel in each grain, and divided by the number of voxels in the grain. Figure 2(b) shows the poor correlation between the calculated and measured ε_{22} values for the first strain state (load 0) without incorporating the residual stresses. As shown in Fig. 2(b), the value of predicted ε_{22} varies from 0.00018 to 0.00022 while the values of measured ε_{22} vary from 0 to 0.0005, which means that the simulation under-predicted ε_{22} at the grain scale.

To improve the correlation between calculated and measured fields, we imposed eigenstrains in each grain calculated with Eq. 10 using the final adjustment factor matrix β following the methodogy of Pokharel and Lebensohn [26] (see appendix A for details):

$$\beta_{ij} = \begin{bmatrix} 1.11 & 0.622 & 1.059 \\ 0.622 & 0.85 & 0.603 \\ 1.059 & 0.603 & 0.925 \end{bmatrix}$$

In the next two sections, we compare the calculated and measured micromechanical fields qualitatively and quantitatively.

5-1 Comparison of Fields Mapped onto 69 Grains Measured by nf-HEDM

Figures 3 and 4 compare the predicted and measured elastic strain and stress fields, respectively, at *load 0* mapped onto the 69 grains measured by nf-HEDM. The figures show that, qualitatively, MASSIF predicted similar patterns of stress and elastic strain at the grain scale compared to those measured by HEDM at *load 0*. As expected, the grains experience the highest value of elastic strain/stress in the loading direction (direction 2). The values of the elastic strains in the direction 1 are higher than those in the direction 3. This is expected, given the observation from Fig. 1(c), that the stiffer crystal c-axis is on average aligned with the direction 3 of the sample. The figures illustrate the development of substantial intergranular heterogeneities in local stresses – including triaxiality – under the application of simple uniaxial loading.

Figures 5 and 6 show the comparison between elastic strain and stress fields, respectively, along the loading direction, measured by HEDM and calculated by MASSIF at the grain scale at *load 1*, *load 2*, and *load 3*. The figures show that different patterns appear in the stress/strain fields in both the calculated and measured fields at different load levels. For example, some grains exhibit hot spots of stress and strain at a lower loading but become cold spots at a higher load level. By contrast, some grains show lower values of stress/strain fields in the initial

loading, but develop higher values of the fields at another load level. These observations reveal the complexity of deformation at the grain scale.

Beyond the pictorial comparison presented in the previous figures, correlation plots between calculated and measured fields in the Ti-7Al HEDM dataset are presented in the next section as a means of quantitative comparison.

5-2 Correlation between Fields Measured by HEDM and Calculated by MASSIF

Figures 7 and 8 show correlation plots between each of the six components of the elastic strain and stress tensors, respectively, as calculated by MASSIF and measured by HEDM at *load 0*. The typical resolution quoted for the ff-HEDM technique is $\pm 10^{-4}$ in strain, which is shown as a horizontal bar on each plot; this scatter is comparable to (and smaller than) the width of the point cloud in each case, which seems reasonable. Again, note that the ff-HEDM measurements are grain-averaged, so the calculated values are also averages over each individual grain. In each figure, the points represent 550 grains in the ff-HEDM dataset, with the actual linear regression line and the perfect correlation ($y=x$) line, which are shown in all plots in blue and red, respectively. We plotted the prediction interval as the purple dash lines in the correlation plots. The interval means the area in which you expect 95 % of all data points to fall. The plots suggest that there are meaningful correlations for all six components at *load 0*, and that the initialization of plastic strain with eigenstrain significantly improved the correlations. However, there are few grains in the plots having the larger deviation from the center of gravity in each correlation plot. For these outlier grains, the predicted and measured components are not in a good agreement. To decrease the effect of outliers on the linear regression estimation, robust regression is an alternative method [35], which iteratively assigns weight to the outlier points to minimize the residual standard error in the fitting. To first order, the weight applied to an individual point is decreased if it strongly affects the slope of the fitted line. As shown in Figs. 7 and 8, the (green) robust regression line, is almost the same as linear regression, indicating that outlier points (grains) do not significantly influence the linear regression at *load 0*.

As mentioned earlier, HEDM experiments measured only the elastic strain components, which means that the stress values were derived quantities using Eq. (11). Consequently, the stress and strain correlation plots are almost the same at *load 0*, as shown in Figs. 7 and 8. Therefore, as a validation of the simulation results, we only compare measured and calculated elastic strain at the subsequent load levels. Figure 9 shows correlation plots between the diagonal component in the loading direction (ε_{22}) and one shear component (ε_{12}) of the elastic strain tensor, as measured by HEDM and calculated by MASSIF for *load 1* to *load 3*. As shown in the correlation plots, the two regression methods predict the same fitted line, and the deviation of the regression line noticeably increases from the y=x line with increasing load. The

actual regression lines track very close to the ideal correlation for *load 1*, at which the grains are still overwhelmingly deforming in the elastic regime. However, the increasing deviation at *load 2* to *load 3* is likely due to an increasing number of grains deforming plastically. The several factors that affect these correlations are discussed in the next section.

6. Discussion

The α-phase titanium alloy Ti-7Al modeled in this work has a hexagonal close packed crystal structure. Residual stresses (at the grain scale) arise during thermomechanical processing because of anisotropic thermal expansion, for example [20,36]. In our formulation, eigenstrains encompass inelastic strains of different origins, such as thermal strains, misfit strains, previous plastic strains or transformation strains. As mentioned in section 4, to consider the initial micromechanical state of the material in our calculations, we used an eigenstrain field to instantiate the measured residual strains. Although this instantiation significantly improved the level of agreement between calculated and measured fields, Fig. 2 shows that the calculated macroscopic stress-strain curve is not sensitive to the addition of an initial eigenstrain field. This is reasonable because, by definition, eigenstrain is a stress-free strain existing under zero applied stress, and the incorporation of eigenstrain does not change the volume average of the stress field.

As described previously, to calculate eigenstrain in each grain, we used an expression involving the Eshelby tensor. The calculated eigenstrain values do not give a perfect correlation between calculated and measured fields at *load 0*, so we used an adjustment factor, described in [26], to optimize the correlation. The imperfect correlations can be the result of several assumptions made in the original Eshelby approximation. According to the latter, eigenstrain values are computed for a spherical inclusion embedded in an infinite homogeneous matrix. However, the shapes of grains deviate from spherical, which introduces deviations from the Eshelby approximation. In addition, our sample is a polycrystalline aggregate, which is neither infinite nor homogeneous. Therefore, the nearest neighbor interactions can be different from those idealized for grains embedded in a homogenous matrix. Furthermore, the finite matrix also can be the source of some adverse effects on the correlations [26].

As mentioned earlier, the correlation between experiment and simulation becomes gradually weaker, and is weakest at *load 3*. The slope of the fitted line can be related to the number of grains deforming plastically at each load level. The amount of slip at each point x strongly depends on the Voce hardening parameters. The adopted initial CRSS's of each slip mode shown in table 2 are in agreement with another study on Ti-7Al [33], which showed that prismatic slip is the easiest slip mode, basal slip activates at a higher stress than prismatic slip,

and pyramidal <c+a> slip is the hardest slip mode among the three modes. The other hardening parameters ($\tau_1, \theta_0, \theta_1$) can only be accurately determined from macroscopic stress-strain behavior beyond the incipient plastic strain reached in the present experiment. Therefore, we adopted the same hardening parameters as in [32]. However, the comparison of results of other experiments/simulations performed on α-phase titanium ([32-34]) show that each slip mode can have different hardening parameters. Consequently, to improve the correlations at *load2,* and especially at *load3*, there is a need to gather more data in the plastic region of the macroscopic stress-strain curve for a more accurate calibration of the hardening parameters. In addition, Pokharel et al. [1] reviewed the literature on comparisons of experimental measurements of texture change at the grain scale with full field crystal plasticity simulations and reached the conclusion that there are no examples of good agreement at the local level. This suggests that further research will be required to attain good agreement at the grain scale and below even when texture development and stress-strain behavior is well matched at the sample scale.

7. Conclusion

We performed a set of fully 3-dimensional elasto-viscoplastic micro-mechanical calculations with the MASSIF code on a voxelized instantiation of a Ti-7Al specimen, which was characterized by far-field and near-field HEDM. The predicted and measured intergranular strain fields developed under tensile loading were compared on a per-grain basis. Excellent agreement was obtained for all components of elastic strain at the first two load states, thereby validating the simulation approach in this regime. Thereafter, the agreement deteriorated as plastic yield was approached, most likely because of highly localized plastic activity and the lack of an accurate enough constitutive description in this deformation regime. The agreement, however, was better for the off-diagonal components of strain than the diagonal components. Initial residual stress played a key role in the accuracy of the calculated results. Without incorporating residual stress in the calculations via an eigenstrain approach, there was no meaningful correlation between the calculated and measured fields at the grain scale, even though the MASSIF simulation was calibrated to reproduce the macroscopic stress-strain curve. This result in particular highlights the critical need for continued polycrystal plasticity model validation using data measured in situ at the intergranular mesoscale.

Acknowledgements

The authors acknowledge support from the PETTT program under the High Performance Computing Modernization Office, and the support of Drs. James Lill and Christopher Woodward in particular are acknowledged. Vahid Tari acknowledges fruitful discussions with Rachel Lim.

Contributions are acknowledged by J. Schuren, R.M. Suter, S.F. Li, P. Kenesei and J. Almer for the measurements at beamline 1ID at the Advanced Photon Source. T.J. Turner and P.A. Shade acknowledge support from the Materials & Manufacturing Directorate of the U.S. Air Force Research Laboratory. This work used the Extreme Science and Engineering Discovery Environment (XSEDE), which is supported by National Science Foundation grant number ACI-1548562. Ricardo Lebensohn acknowledges support from DOE-DoD Joint Munitions Program and LANL's Mesoscale Science Outreach, Momentum Initiative. The work of J.V. Bernier was performed under the auspices of the U.S. Department of Energy by Lawrence Livermore National Laboratory under Contract DE-AC52-07NA27344.

Appendix A

Calculation steps for β_{ij} :

1. In each grain, use the Eshelby approximation (Eq. A.1) to calculate the eigenstrain from the measured initial elastic strain.

$$\varepsilon_{ij}^{*,g} = (S_{ijkl} - I_{ijkl})^{-1}\varepsilon_{kl}^{r,g} \quad \text{A.1}$$

Here $\varepsilon_{ij}^{*,g}$, $\varepsilon_{kl}^{r,g}$, S_{ijkl}, and I_{ijkl} are the eigenstrain, initial residual elastic strain, Eshelby tensor, and fourth-rank identity matrix, respectively.

2. Instantiate MASSIF calculation using the eigenstrain calculated with Eq. A.1

$$\varepsilon_{ij}(x) = \varepsilon_{ij}^{e}(x) + \varepsilon_{ij}^{p}(x) + \varepsilon_{ij}^{*}(x) = C_{ijkl}^{-1}(x)\sigma_{kl}(x) + \varepsilon_{ij}^{p,t}(x) + \dot{\varepsilon}_{ij}^{p}(x,\sigma)\Delta t + \varepsilon_{ij}^{*}(x) \quad \text{A.2}$$

The details of Eq. A.2 are described in the manuscript (Eq. 1 and Eq.6). Figure A.1 shows the correlation plots for each of the six elastic strain components calculated by MASSIF, based on the Eshelby approximation (Eq. A.1), compared with the values measured by ff-HEDM in each grain at load 0.

3. Calculate the β_{ij}

As shown in figure A.1 based on the Eshleby approximation (Eq. A.1), the correlation plots show deviations of the linear regression (blue lines) from the ideal one-to-one correlation (red lines). To bring the calculated strain values closer to the ideal one-to-one correlation

lines, i.e., improve the correlation, an adjustment factor β_{ij} is calculated as the inverse of the slope of the regression line for each component. Table A.1 lists the values of β_{ij} and slope from linear regression for all six components.

Table A.1: Slope and y-intercept values from the linear regression for each elastic strain component at load 0, calculated by MASSIF based on the Eshelby approximation (Eq. A.1) and the values measured by ff-HEDM. Each adjustment factor β_{ij} is the inverse of slope of the corresponding regression line in figure A.1.

ε_{ij}	ε_{11}	ε_{22}	ε_{33}	ε_{12}	ε_{13}	ε_{23}
Slope m_{ij}	0.902	1.177	1.077	1.607	0.944	1.659
y-intercept	$-1.58e^{-04}$	$-1.49e^{-04}$	$-2.13e^{-05}$	$-6.71e^{-05}$	$-2.51e^{-06}$	$-1.83e^{-05}$
Adjustment factor β_{ij}	1.11	0.85	0.925	0.622	1.059	6.03

4. Calculate adjusted eigenstrain values (Eq. A.3) by using the adjustment factors β_{ij} (Table A.1)

$$\varepsilon_{ij}^{*,g} = \beta_{ij}(S_{ijkl} - I_{ijkl})^{-1}\varepsilon_{kl}^{r,g} \qquad \text{(no sum over ij)} \qquad \text{A.3}$$

5. Instantiate the MASSIF calculation by using the new eigenstrain values calculated with Eq. A.3.

Figure 7 in the manuscript shows the new correlation plots between calculated and measured values at load 0, after adjusting the eigenstrain using Eq. A.3 with the numerical values of β_{ij} given in Table A.1.

References

[1] R. Pokharel, J. Lind, A.K. Kanjarla, R.A. Lebensohn, S.F. Li, P. Kenesei, R.M. Suter, A.D. Rollett, Polycrystal Plasticity: Comparison Between Grain - Scale Observations of Deformation and Simulations, Annu. Rev. Condens. Matter Phys. 5 (2014) 317–346.
[2] C. Efstathiou, H. Sehitoglu, J. Lambros, Multiscale strain measurements of plastically deforming polycrystalline titanium: Role of deformation heterogeneities, Int. J. Plast. 26 (2010) 93–106.
[3] E. Pouillier, A.-F. Gourgues, D. Tanguy, E.P. Busso, A study of intergranular fracture in an aluminium alloy due to hydrogen embrittlement, Int. J. Plast. 34 (2012) 139–153.
[4] C. Niederberger, W.M. Mook, X. Maeder, J. Michler, In situ electron backscatter diffraction (EBSD) during the compression of micropillars, Mater. Sci. Eng. A. 527 (2010) 4306–4311.
[5] L. Delannay, M.R. Barnett, Modelling the combined effect of grain size and grain shape on plastic anisotropy of metals, Int. J. Plast. 32–33 (2012) 70–84.
[6] D. Raabe, M. Sachtleber, Z. Zhao, F. Roters, S. Zaefferer, Micromechanical and macromechanical effects in grain scale polycrystal plasticity experimentation and simulation, Acta Mater. 49 (2001) 3433–3441.
[7] V. Tari, A.D. Rollett, H.E. Kadiri, H. Beladi, A.L. Oppedal, R.L. King, The effect of deformation twinning on stress localization in a three dimensional TWIP steel microstructure, Model. Simul. Mater. Sci. Eng. 23 (2015) 45010.
[8] C. Zhang, H. Li, P. Eisenlohr, W. Liu, C.J. Boehlert, M.A. Crimp, T.R. Bieler, Effect of realistic 3D microstructure in crystal plasticity finite element analysis of polycrystalline Ti-5Al-2.5Sn, Int. J. Plast. 69 (2015) 21–35.
[9] T.J. Turner, P.A. Shade, J.C. Schuren, M.A. Groeber, The influence of microstructure on surface strain distributions in a nickel micro-tension specimen, Model. Simul. Mater. Sci. Eng. 21 (2013) 15002.
[10] P.A. Shade, M.A. Groeber, J.C. Schuren, M.D. Uchic, Experimental measurement of surface strains and local lattice rotations combined with 3D microstructure reconstruction from deformed polycrystalline ensembles at the micro-scale, Integrating Mater. Manuf. Innov. 2 (2013) 5.
[11] J.C. Schuren, P.A. Shade, J.V. Bernier, S.F. Li, B. Blank, J. Lind, P. Kenesei, U. Lienert, R.M. Suter, T.J. Turner, D.M. Dimiduk, J. Almer, New opportunities for quantitative tracking of polycrystal responses in three dimensions, Curr. Opin. Solid State Mater. Sci. 19 (2015) 235–244.
[12] U. Lienert, S.F. Li, C.M. Hefferan, J. Lind, R.M. Suter, J.V. Bernier, N.R. Barton, M.C. Brandes, M.J. Mills, M.P. Miller, B. Jakobsen, W. Pantleon, High-energy diffraction microscopy at the advanced photon source, JOM. 63 (2011) 70–77.
[13] S.F. Li, J. Lind, C.M. Hefferan, R. Pokharel, U. Lienert, A.D. Rollett, R.M. Suter, Three-dimensional plastic response in polycrystalline copper via near-field high-energy X-ray diffraction microscopy, J. Appl. Crystallogr. 45 (2012) 1098–1108.
[14] H.F. Poulsen, S.F. Nielsen, E.M. Lauridsen, S. Schmidt, R.M. Suter, U. Lienert, L. Margulies, T. Lorentzen, D. Juul Jensen, Three-dimensional maps of grain boundaries and the stress

state of individual grains in polycrystals and powders, J. Appl. Crystallogr. 34 (2001) 751–756.
[15] J.V. Bernier, N.R. Barton, U. Lienert, M.P. Miller, Far-field high-energy diffraction microscopy: a tool for intergranular orientation and strain analysis, J. Strain Anal. Eng. Des. 46 (2011) 527–547.
[16] J. Oddershede, S. Schmidt, H.F. Poulsen, H.O. Sørensen, J. Wright, W. Reimers, Determining grain resolved stresses in polycrystalline materials using three-dimensional X-ray diffraction, J. Appl. Crystallogr. 43 (2010) 539–549.
[17] S.F. Li, R.M. Suter, Adaptive reconstruction method for three-dimensional orientation imaging, J. Appl. Crystallogr. 46 (2013) 512–524.
[18] R.M. Suter, D. Hennessy, C. Xiao, U. Lienert, Forward modeling method for microstructure reconstruction using x-ray diffraction microscopy: Single-crystal verification, Rev. Sci. Instrum. 77 (2006) 123905. doi:10.1063/1.2400017.
[19] T.J. Turner, P.A. Shade, J.V. Bernier, S.F. Li, J.C. Schuren, P. Kenesei, R.M. Suter, J. Almer, Crystal Plasticity Model Validation Using Combined High-Energy Diffraction Microscopy Data for a Ti-7Al Specimen, Metall. Mater. Trans. A. 48 (2017) 627–647.
[20] W. Boas, R.W. Honeycombe, Thermal fatigue of metals, Nature. 153 (1944) 494–495.
[21] K. Chatterjee, A. Venkataraman, T. Garbaciak, J. Rotella, M.D. Sangid, A.J. Beaudoin, P. Kenesei, J.-S. Park, A.L. Pilchak, Study of grain-level deformation and residual stresses in Ti-7Al under combined bending and tension using high energy diffraction microscopy (HEDM), Int. J. Solids Struct. 94–95 (2016) 35–49. doi:10.1016/j.ijsolstr.2016.05.010.
[22] D. Naragani, M.D. Sangid, P.A. Shade, J.C. Schuren, H. Sharma, J.-S. Park, P. Kenesei, J.V. Bernier, T.J. Turner, I. Parr, Investigation of fatigue crack initiation from a non-metallic inclusion via high energy x-ray diffraction microscopy, Acta Mater. 137 (2017) 71–84. doi:10.1016/j.actamat.2017.07.027.
[23] T.J. Turner, P.A. Shade, J.V. Bernier, S.F. Li, J.C. Schuren, J. Lind, U. Lienert, P. Kenesei, R.M. Suter, B. Blank, J. Almer, Combined near- and far-field high-energy diffraction microscopy dataset for Ti-7Al tensile specimen elastically loaded in situ, Integrating Mater. Manuf. Innov. 5 (2016) 5.
[24] R.A. Lebensohn, A.K. Kanjarla, P. Eisenlohr, An elasto-viscoplastic formulation based on fast Fourier transforms for the prediction of micromechanical fields in polycrystalline materials, Int. J. Plast. 32–33 (2012) 59–69.
[25] HDF Home, HDF Group. (n.d.). https://www.hdfgroup.org/ (accessed November 12, 2017).
[26] R. Pokharel, R.A. Lebensohn, Instantiation of crystal plasticity simulations for micromechanical modelling with direct input from microstructural data collected at light sources, Scr. Mater. 132 (2017) 73–77.
[27] E.J. Lieberman, R.A. Lebensohn, D.B. Menasche, C.A. Bronkhorst, A.D. Rollett, Microstructural effects on damage evolution in shocked copper polycrystals, Acta Mater. 116 (2016) 270–280. doi:10.1016/j.actamat.2016.06.054.
[28] H. Moulinec, P. Suquet, A numerical method for computing the overall response of nonlinear composites with complex microstructure, Comput. Methods Appl. Mech. Eng. 157 (1998) 69–94.

[29] J.C. Michel, H. Moulinec, P. Suquet, A computational method based on augmented lagrangians and fast fourier transforms for composites with high contrast, CMES - Comput. Model. Eng. Sci. 1 (2000) 79–88.
[30] R.A. Lebensohn, R. Brenner, O. Castelnau, A.D. Rollett, Orientation image-based micromechanical modelling of subgrain texture evolution in polycrystalline copper, Acta Mater. 56 (2008) 3914–3926. doi:10.1016/j.actamat.2008.04.016.
[31] A.D. Rollett, R.A. Lebensohn, M. Groeber, Y. Choi, J. Li, G.S. Rohrer, Stress hot spots in viscoplastic deformation of polycrystals, Model. Simul. Mater. Sci. Eng. 18 (2010) 74005. doi:10.1088/0965-0393/18/7/074005.
[32] R.A. Lebensohn, P.A. Turner, J.W. Signorelli, G.R. Canova, C.N. Tomé, Calculation of intergranular stresses based on a large-strain viscoplastic self-consistent polycrystal model, Model. Simul. Mater. Sci. Eng. 6 (1998) 447.
[33] E.S. Fisher, C.J. Renken, Single-Crystal Elastic Moduli and the hcp → bcc Transformation in Ti, Zr, and Hf, Phys. Rev. 135 (1964) A482–A494.
[34] D.C. Pagan, P.A. Shade, N.R. Barton, J.-S. Park, P. Kenesei, D.B. Menasche, J.V. Bernier, Modeling slip system strength evolution in Ti-7Al informed by in-situ grain stress measurements, Acta Mater. 128 (2017) 406–417. doi:10.1016/j.actamat.2017.02.042.
[35] D.C. Hoaglin, F. Mosteller, J.W. Tukey, eds., Exploring Data Tables, Trends, and Shapes, Revised edition, Wiley-Interscience, Hoboken, NJ, 2006.
[36] R.R. Pawar, V.T. Deshpande, The anisotropy of the thermal expansion of α-titanium, Acta Crystallogr. A. 24 (1968) 316–317.

Table 1: Elastic constants used in MASSIF simulation [33]

	C_{11}	C_{12}	C_{13}	C_{33}	C_{44}	C_{66}
Values in GPa	162.4	92	69	180.7	46.7	35.2

Table 2: Voce hardening parameters for different slip modes

Slip modes	τ_0(MPa)	τ_1(MPa)	θ_0(MPa)	θ_1(Mpa)
Prismatic	220	5	35	30
Basal	245	5	35	30
Pyramidal <c+a>	388	5	35	30

Figure captions

Fig. 1. (a) (0001) pole figure for grains based on the far field HEDM measurements. (b) Voronoi tessellation for representation of ff-HEDM data containing 550 grains; (c) a set of 69 grains in the middle plane of Fig. 1b measured by near field HEDM, with color based on the grain identification number.

Fig. 2. (a) measured macroscopic stress-strain responses, and stress-strain curves calculated by MASSIF under uniaxial tension, (b) correlation at *load 0*, i.e., the initial load state, between the e_{22} component measured by HEDM and calculated by MASSIF at grain scale for 550 grains without eigenstrain calculation of the initial residual stress state. The red line corresponds to a one-to-one correlation and the blue line to the result of linear regression, clearly indicating that the calculated response does not correspond to the measurements.

Fig. 3. Elastic strain for the set of 69 grains at load 0, comparing values of each leading diagonal component measured by HEDM with those calculated by MASSIF. Note that in this and all succeeding figures, eigenstrain instantiation of the initial residual stress state was used.

Fig. 4. Stress for the set of 69 grains at load 0, comparing values of each leading diagonal component deduced from HEDM measurements with those calculated by MASSIF.

Fig. 5. Elastic strain for the set of 69 grains, comparing values of e_{22} measured by HEDM and those calculated by MASSIF at load 1, load 2, and load 3.

Fig. 6. Stress for the set of 69 grains, comparing values of σ_{22} measured by HEDM and those calculated by MASSIF at load 1, load 2, and load 3.

Fig. 7. Correlation plots for all six elastic strain components as calculated by MASSIF versus measured by HEDM for 550 grains at load 0. The red line is the desired one-to-one correlation. The results of linear and robust regression are both close to one-to-one. The purple dash lines represent the prediction interval (PI). The expected 10-4 resolution (in strain) for the ff-HEDM is indicated by a dumbbell in the lower left corner of each plot.

Fig. 8. Correlation plots for each stress component as calculated by MASSIF versus deduced by HEDM for 550 grains at load 0. The red line is the ideal correlation. The results of linear and robust regression are both close to the ideal correlation. The purple dash lines represent the prediction interval (PI).

Fig. 9. Correlation plots for two elastic strain components as calculated by MASSIF versus measured by HEDM for 550 grains at load 1, load 2, and load 3. The strain values in the loading direction (2) increase whereas the shear component remains centered on zero. The red line is the desired one-to-one correlation; the blue line represents a conventional least squares fit whereas the green line represents a robust regression that minimizes the influence of the outliers and, in most cases, is close to the (red) one-to-one line. The purple dash lines represent the prediction interval (PI).

Fig. A.1 Correlation plots for all six elastic strain components as calculated by MASSIF versus measured by HEDM for 550 grains at load 0 based on Eshelby's approximation (Eq. A.1)

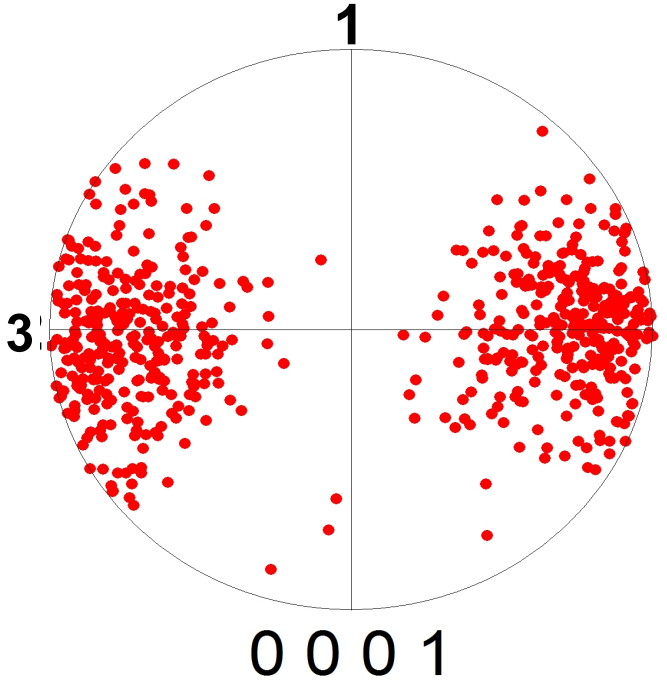

(a)

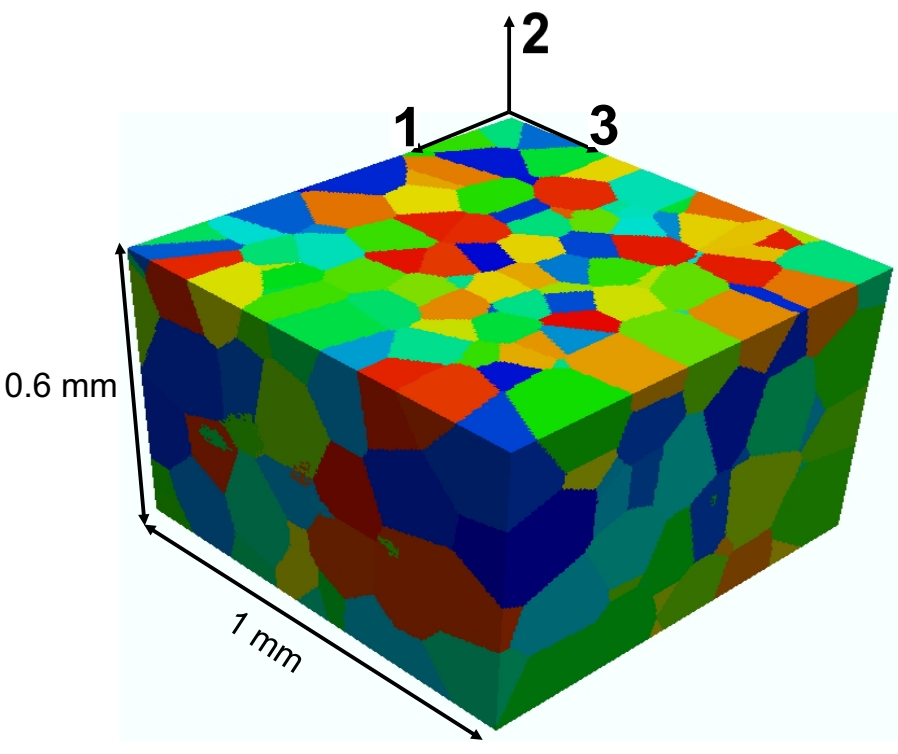

(b)

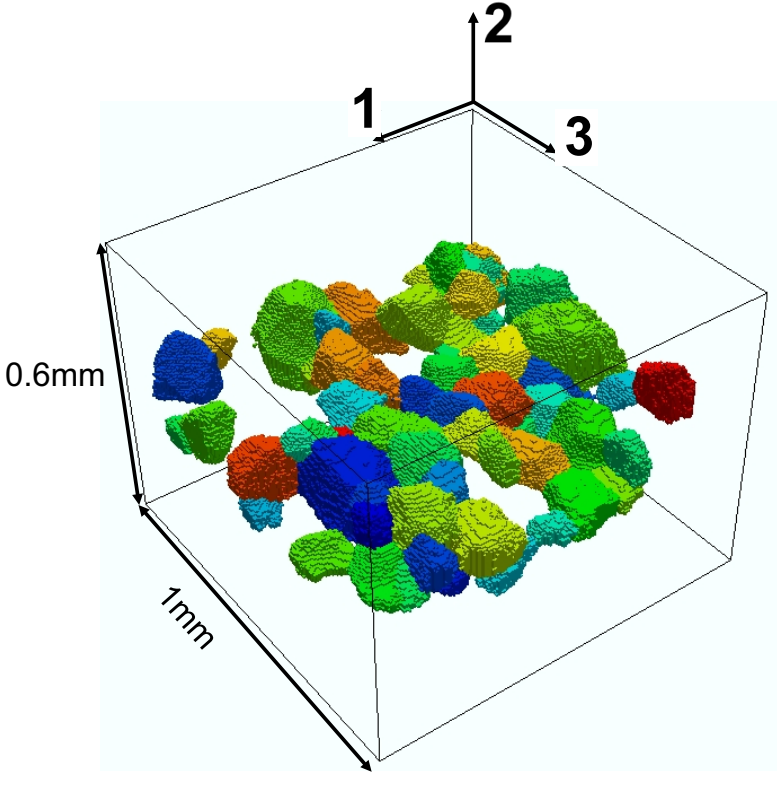

(c)

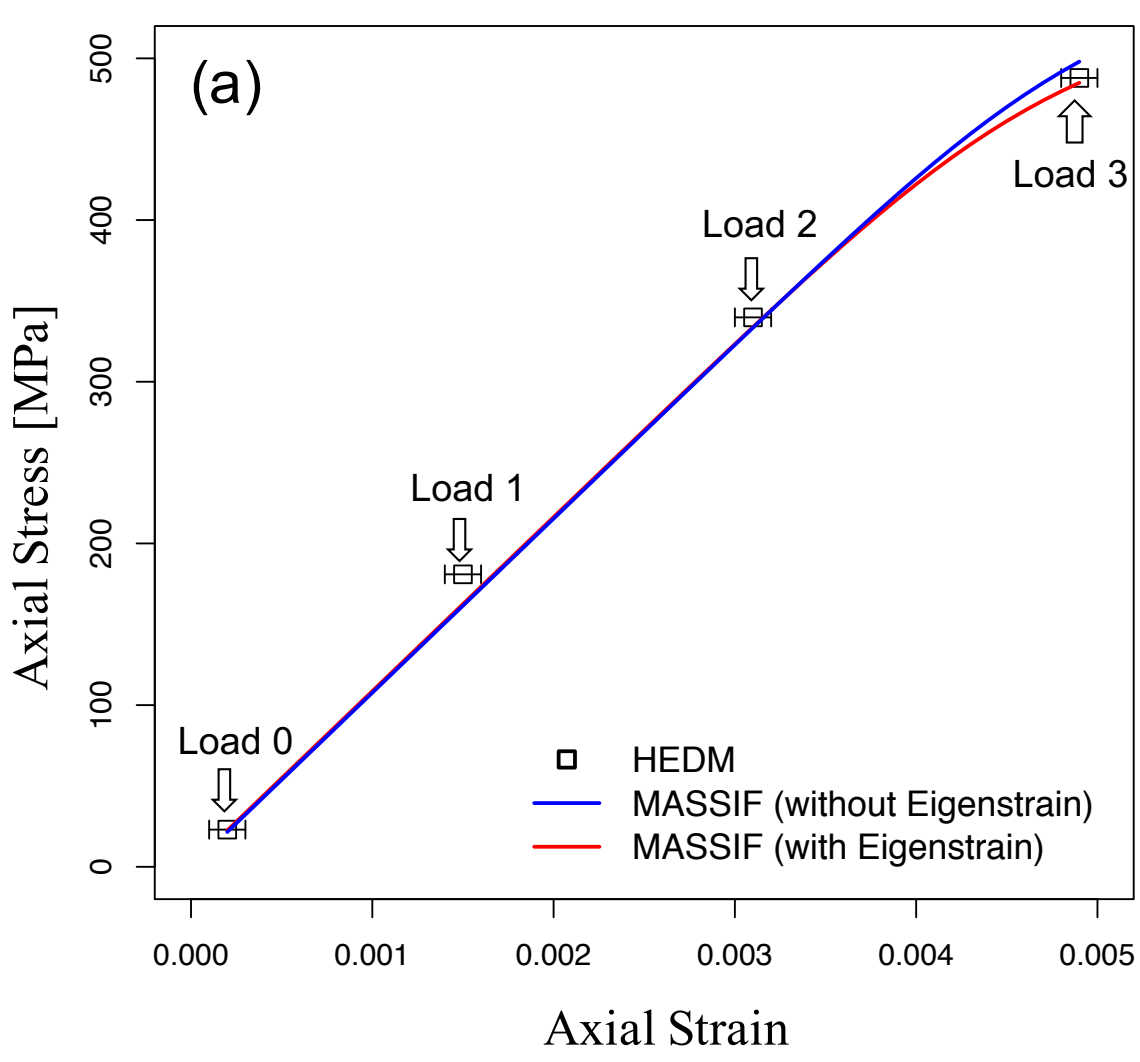
(a)
Load 0
Load 1
Load 2
Load 3
HEDM
MASSIF (without Eigenstrain)
MASSIF (with Eigenstrain)
Axial Stress [MPa]
Axial Strain
0
100
200
300
400
500
0.000
0.001
0.002
0.003
0.004
0.005

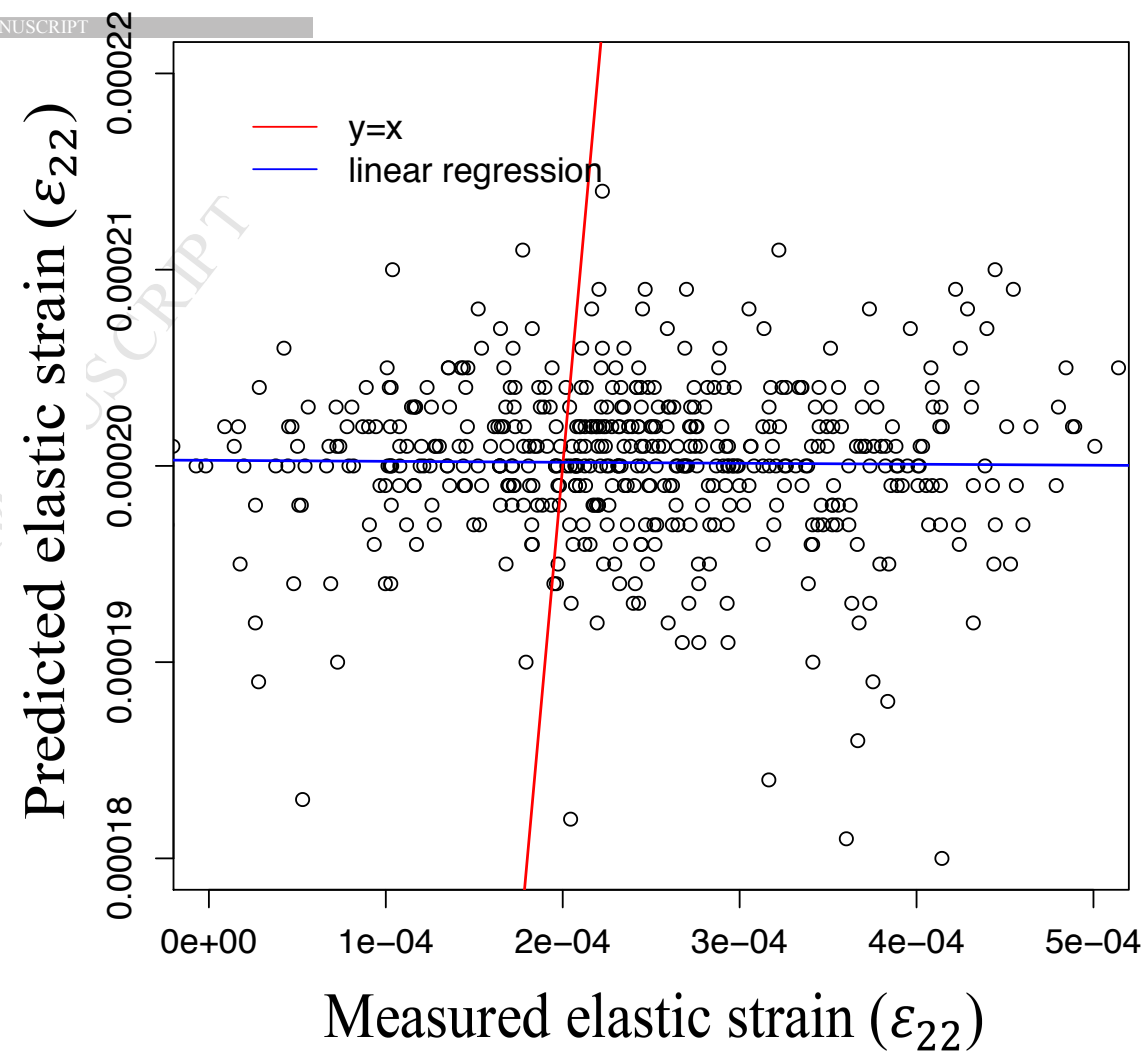
y=x
linear regression
Predicted elastic strain (ε_{22})
Measured elastic strain (ε_{22})
0.00018
0.00019
0.00020
0.00021
0.00022
0e+00
1e−04
2e−04
3e−04
4e−04
5e−04

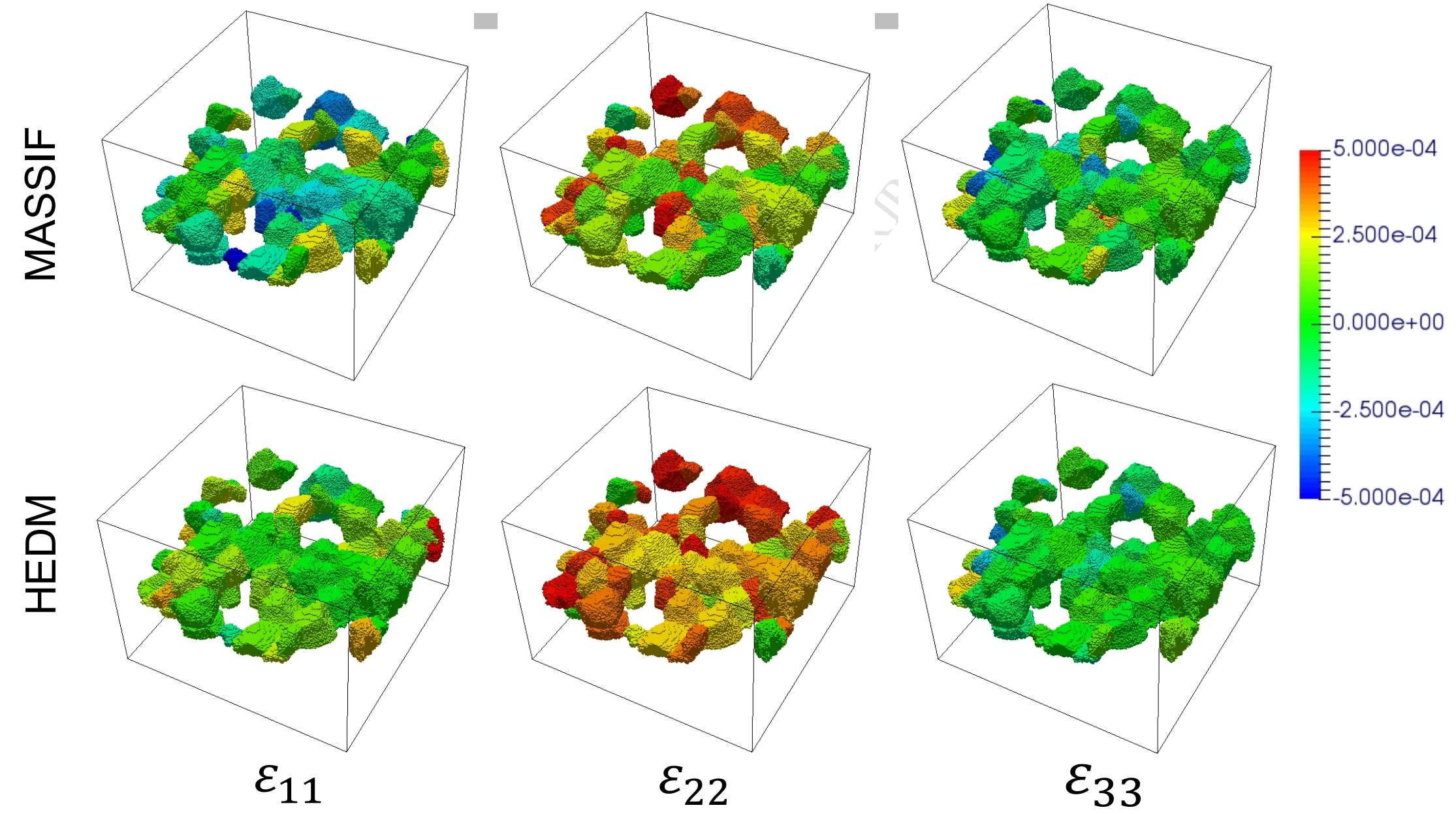
MASSIF
HEDM
5.000e-04
2.500e-04
0.000e+00
-2.500e-04
-5.000e-04
ε_{11}
ε_{22}
ε_{33}

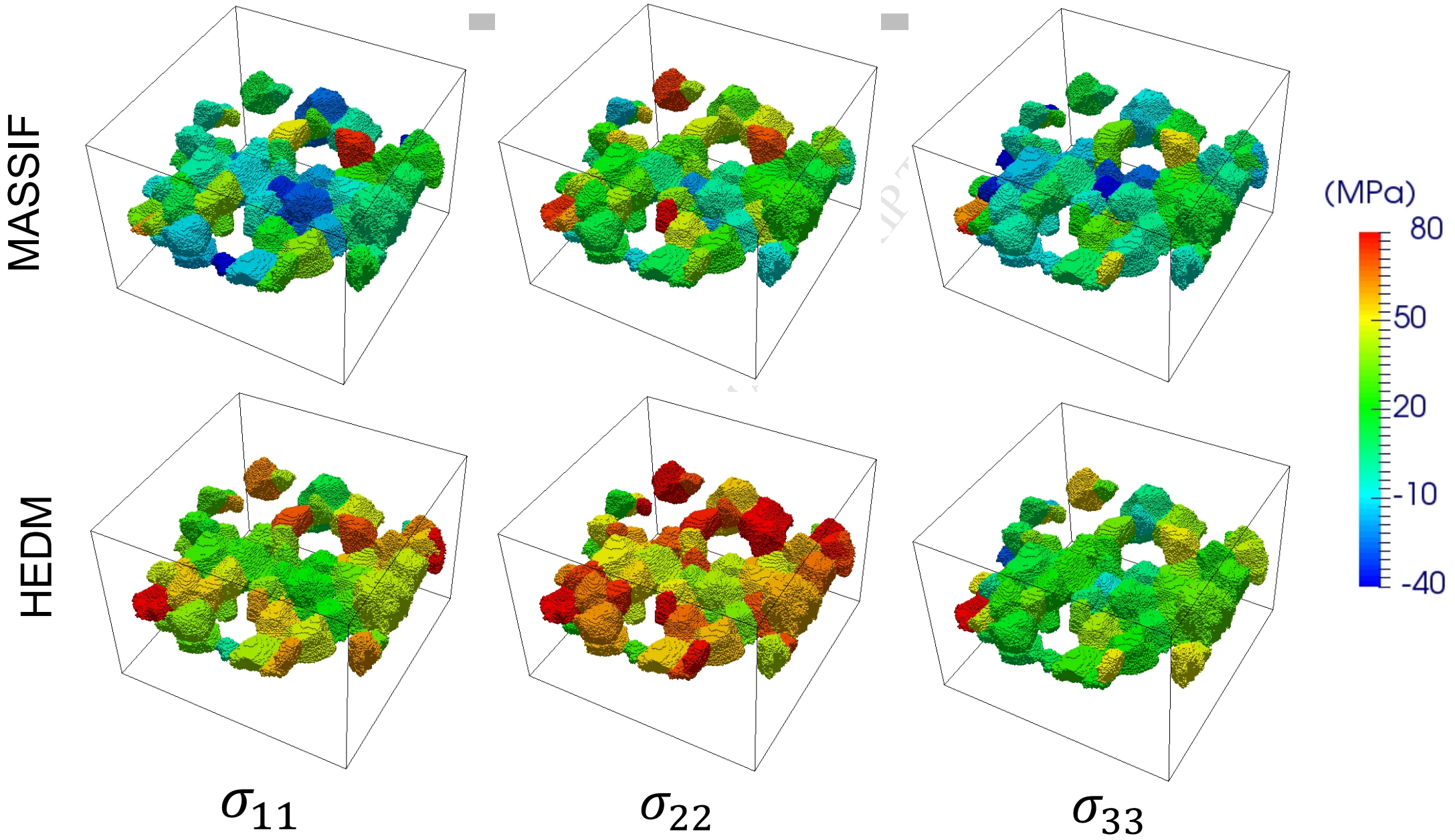
MASSIF
HEDM
(MPa)
80
50
20
-10
-40
σ_{11}
σ_{22}
σ_{33}

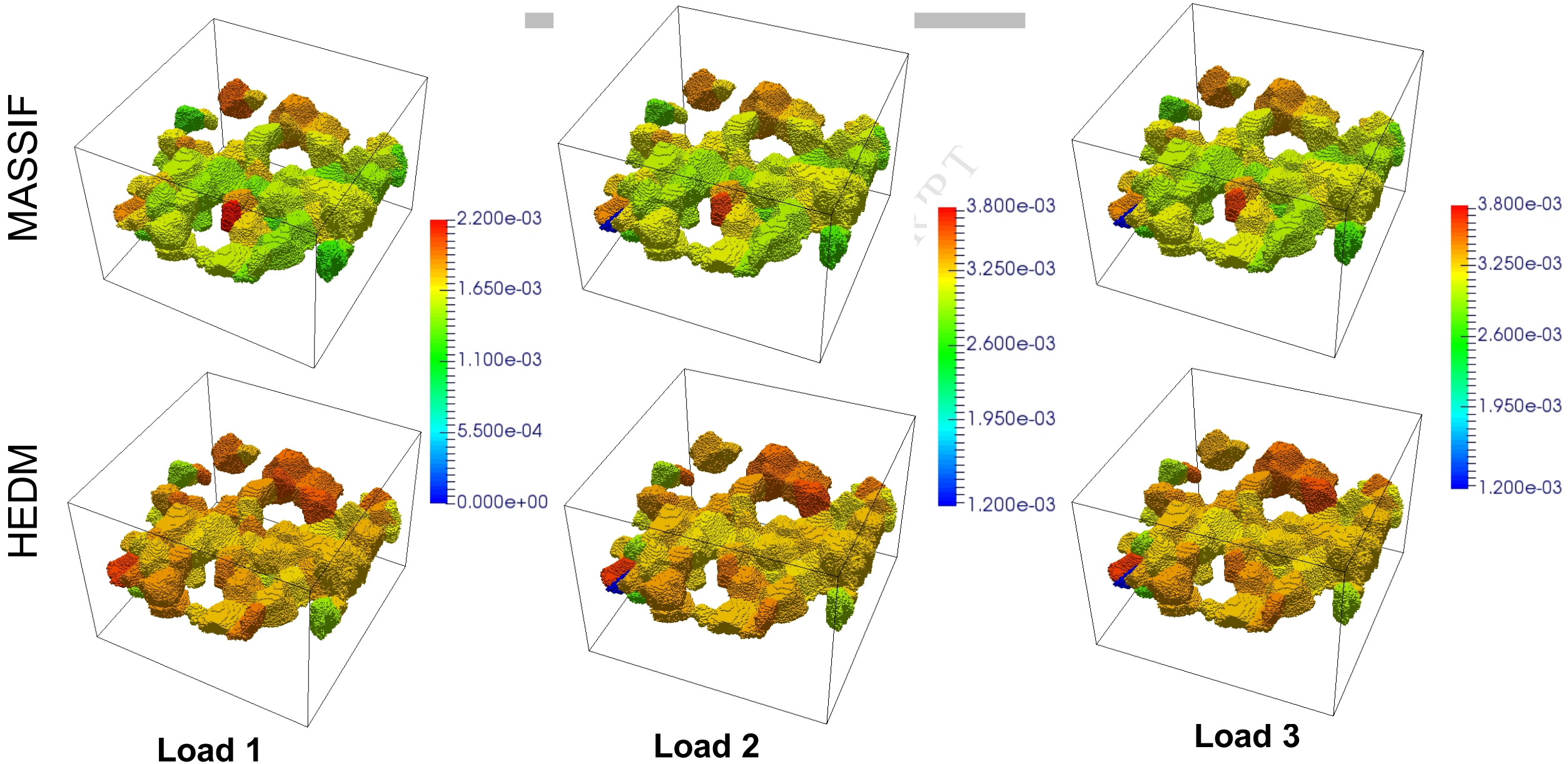
MASSIF
HEDM
2.200e-03
1.650e-03
1.100e-03
5.500e-04
0.000e+00
3.800e-03
3.250e-03
2.600e-03
1.950e-03
1.200e-03
3.800e-03
3.250e-03
2.600e-03
1.950e-03
1.200e-03
Load 1
Load 2
Load 3

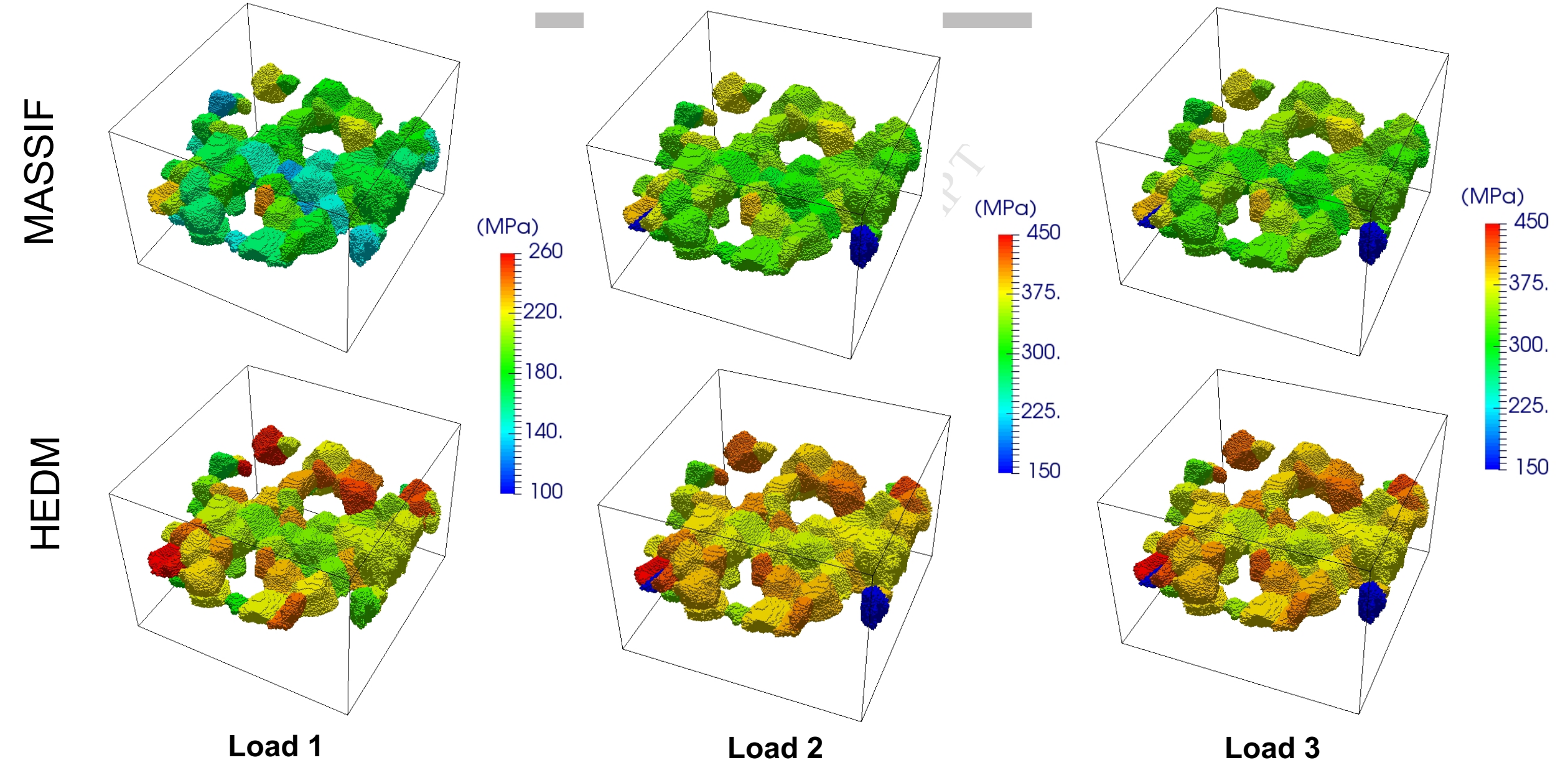
MASSIF
HEDM
(MPa)
260
220.
180.
140.
100
(MPa)
450
375.
300.
225.
150
(MPa)
450
375.
300.
225.
150
Load 1
Load 2
Load 3